Available online at www.sciencedirect.com
ScienceDirect
Journal of Computational Physics 221 (2007) 524–538
JOURNAL OF COMPUTATIONAL PHYSICS
www.elsevier.com/locate/jcp

On the finite volume discretization of discontinuous body force field on collocated grid: Application to VOF method

Jure Mencinger *, Iztok Žun

Laboratory of Fluid Dynamics and Thermodynamics, Faculty of Mechanical Engineering, University of Ljubljana, Aškerčeva 6, 1000 Ljubljana, Slovenia

Received 14 March 2006; received in revised form 15 June 2006; accepted 18 June 2006
Available online 14 August 2006

Abstract

Discontinuities in the body force field typically appear at the interface of two fluid systems. Modeled with the volume-of-fluid (VOF) and discretized with the finite volume method, the discontinuous body force fields are represented as abruptly variable. In the present study, gravity and continuum surface force (CSF) are considered. Such strongly variable body forces can produce unphysical spikes in the velocity field when collocated variable arrangement is used. The spikes can be eliminated following a force field discretization rule which is deduced by imposing a constraint requiring a zero velocity solution when the forces applied to the system are equilibrated with the gradient of the pressure field. It is shown (as a byproduct of the present work) that a zero velocity solution can only be obtained if the force field is conservative on the discrete level, which applies also for the studied case of a stationary bubble. Finally, the case of a rising bubble demonstrates that the proposed rule should be obeyed generally although it is obtained for a quiescent fluid.

Keywords: Collocated grid; Body force; Volume-of-fluid; Continuum surface force; Parasitic currents

1. Introduction

It appears that for engineering applications the benefits of collocated pressure and velocity field arrangement outweigh the drawbacks, as it is used in the majority of today's commercial CFD codes. Its main advantage over the staggered arrangement lies in its easier implementation on non-orthogonal grids. On the other hand, its main disadvantage is that it does not *inherently* ensure strong pressure–velocity coupling, thus allowing for the appearance of a non-physical checkerboard pressure field (e.g., see [1], pp. 198). The most widely used remedy on a collocated grid is the interpolation scheme of Rhie and Chow [2]. Several improvements to this scheme have been suggested by Majumdar [3], Choi [4], Papageorgakopoulos *et al.* [5], Yu *et al.* [6] to name a few. Gu [7] and later Choi *et al.* [8] propose additional corrections for the calculation of flows with large body forces.

* Corresponding author.
E-mail address: Jure.Mencinger@fs.uni-lj.si (J. Mencinger).

0021-9991/$ - see front matter
doi:10.1016/j.jcp.2006.06.021

The Rhie–Chow interpolation yields satisfactory results as long as the pressure field p is sufficiently smooth, which is a rarely met condition in a multiphase system due to the discontinuities in body force fields. Two kinds of discontinuous body force fields are most commonly encountered when dealing with multiple phases:

(1) In the gravity field $\mathbf{g}$, a $(\rho_2 - \rho_1)\mathbf{g}$ jump in body force field $\mathbf{f}_g = \rho\mathbf{g}$ exists on the interface between the two fluids where ρ_1 and ρ_2 are their densities.
(2) Taking into account also the surface energy, the force per unit interfacial area $\mathbf{F}_\sigma = \sigma\kappa\hat{\mathbf{n}}$ is present where σ, κ and $\hat{\mathbf{n}}$ are the surface tension coefficient, the interface curvature and the interface normal, respectively. This surface force $\mathbf{F}_\sigma$ is not convenient for an interface capturing multiphase flow simulation; as shown by Brackbill *et al.* [9] it can be replaced with a body force field $\mathbf{f}_\sigma = \mathbf{F}_\sigma\delta(\hat{\mathbf{n}}(\mathbf{x}_s)\cdot(\mathbf{x} - \mathbf{x}_s))$ where $\delta(x)$ is Dirac's delta function[1] and $\mathbf{x}_s$ is a point on the interface.

Whereas the step in $\mathbf{f}_g$ causes the discontinuity of the ∇p-field, $\mathbf{f}_\sigma$ results in a pressure jump $\Delta p = \sigma\kappa$ at the interface between the two fluids.

For this study we refer to the two phase volume-of-fluid (VOF) model [10] which is based on the concept of fractional volume of fluid denoted by C. Accordingly, the aforementioned body force fields are written as $\mathbf{f}_g = (\rho_1 + C(\rho_2 - \rho_1))\mathbf{g}$ and, using the continuum surface force (CSF) model by Brackbill *et al.* [9], $\mathbf{f}_\sigma = \sigma\kappa\nabla C$. *We consider an ideal VOF simulation without the numerical diffusion of C so that the interface thickness is within one cell size and without the need to mollify C for the calculation of the CSF unless stated otherwise.* Hence, the discretization of $\mathbf{f}_g$ or $\mathbf{f}_\sigma$ results in an abruptly variable discrete field. From a discrete point of view there is no difference between the fields that are either continuous or discontinuous on the continuum scale. Naturally, a discrete field with an abrupt variation can also originate from a corresponding continuous field; in this case the steepness of the variation between the neighboring cells can simply be reduced by grid refinement. On the other hand, when the abruptness originates from discontinuity it persists regardless of the grid density.

The use of the Rhie–Chow interpolation in a VOF-based simulation can result in the appearance of unphysical spikes in the pressure and velocity fields near the interface, as shown later in the paper. Surprisingly, to the authors' knowledge, this issue has not been addressed properly even though the VOF model implementation on collocated grids is used in many applications for both academic and industrial purposes. This is perhaps because the spikes are either attributed to the inaccurate calculation of κ or diminished by the interface smearing resulting from the numerical diffusion of C.

A logical cure for the unphysical spikes would be switching off the Rhie–Chow interpolation on the faces of the cells containing the interface. However, this leads to pressure–velocity decoupling and consequently an unphysical pressure field. Instead we look for the remedy in more suitable discretization of the body force field which causes the discontinuities in the pressure field.

To find a suitable finite volume discretization of body force fields which would suppress the aforementioned spikes, we consider an initially quiescent fluid subject to equilibrated body force field. We impose that the discretization should comply with the exact balance between the body force and the pressure gradient so that $\nabla p = \mathbf{f}$ holds both inside the cells and on the cell faces. Then also the velocity field $\mathbf{u}$ discrete solution must equal zero in all cells and their faces. This rather elementary demand gives a simple, physically comprehensible rule for the discretization of the body force field.

The paper is organized as follows: the Rhie–Chow interpolation scheme and its enhancements are briefly summarized in the next section. Section 3 contains a one-dimensional study of discontinuous force fields acting on a stagnant fluid. The study results in the force field discretization rule. The two-dimensional situation is considered in Section 4; it is also shown that a $\mathbf{u} = 0$ solution to round-off error can only be obtained if the body force field is *conservative on a discrete level*. This is tested on the problem of the parasitic currents appearing at the interface of a stationary bubble [11] – a problem which is more directly connected with the discretization of the CSF. In Section 5 the proposed rule is compared to standard FV force discretization for the case of a rising bubble. Conclusions are given in Section 6.

[1] Strictly mathematically, Dirac's $\delta(x)$ is not a function but a distribution and the term (dis)continuous does not apply. Nevertheless, $\mathbf{f}_s$ is not a continuous field.

2. The Rhie–Chow interpolation and its corrections

This section contains a brief explanation of the Rhie–Chow interpolation; even though it can be found in several CFD textbooks it is useful for easier reference in the following sections and also to introduce some notation used in this paper. We start by writing down the x-component of the momentum equation for an incompressible fluid with constant viscosity η

$$\rho\left(\frac{\partial u}{\partial t}+(\mathbf{u}\cdot\nabla)u\right)=-\frac{\partial p}{\partial x}+\eta\nabla^2 u+f^x, \tag{1}$$

where t, ρ, p, u and f^x are time, fluid density, pressure, x-components of velocity and of body force, respectively. Standard finite volume (FV) discretization (e.g., see [1]) of (1) on a fixed grid results in

$$\left.\frac{\partial(\rho u)}{\partial t}\right|_P V_P+\sum_f F_f u_f=-\left.\frac{\partial p}{\partial x}\right|_P V_P+\sum_f \eta_f\left.\frac{\partial u}{\partial x}\right|_f+f_P^x V_P, \tag{2}$$

where V_P denotes the size of the FV under consideration. The subscripts P and f denote the average values in FV and on FV face, respectively, and the summation comprises all FV faces. In (2), $F_f=\rho_f\mathbf{u}_f\cdot\mathbf{S}_f$ presents mass flux through fth face with its surface vector $\mathbf{S}_f=S_f\hat{\mathbf{n}}_f$ where S_f is the surface and $\hat{\mathbf{n}}$ the normal vector pointing out of the FV. For the incompressible fluid

$$\sum_f F_f=0, \tag{3}$$

follows from the mass conservation expressed with $\nabla\cdot\mathbf{u}=0$.

Because we are concerned with discretization in space, the choice of the time discretization is not essential for the matter at hand. At any rate, we use fully implicit time discretization because of its relative robustness and easy implementation. Pressure and velocity field are coupled via the SIMPLE algorithm [12] which essentially requires solving (2) and (3) repeatedly in succession inside the timestep Δt.

For simplicity, we consider a two-dimensional Cartesian grid; if the FV face values are approximated from those of the neighboring FVs sharing the face then (2) can be written as

$$a_P u_P=a_E u_E+a_W u_W+a_N u_N+a_S u_S+t_P u_P^0+f_P^x V_P-\left.\frac{\partial p}{\partial x}\right|_P V_P, \tag{4}$$

where the subscripts denoting the values the neighboring FVs correspond to standard compass notation [1] (refer also to Fig. 5) and superscript 0 marks the value from previous timestep. If the linear interpolation (CDS) is used to obtain the values on FV faces denoted by lower-case letters e, w, n and s then the coefficients in (4) equal

$$\begin{aligned} &a_E=\frac{\eta_e S_e}{\Delta x_e}+I_e F_e, \quad a_W=\frac{\eta_w S_w}{\Delta x_w}+I_w F_w, \quad a_N=\frac{\eta_n S_n}{\Delta y_n}+I_n F_n,\\ &a_S=\frac{\eta_s S_s}{\Delta y_s}+I_s F_s, \quad t_P=\frac{\rho_P V_P}{\Delta t}, \qquad a_P=a_E+a_W+a_N+a_S+t_P, \end{aligned} \tag{5}$$

where e.g. $\Delta x_e=x_E-x_P$ and $I_e=(x_e-x_P)/\Delta x_e$ denote the distance between points E and P and the linear interpolation coefficient on the corresponding e-face, respectively. The derivative $(\partial p/\partial x)_P$ in (4) is discretized as $(p_e S_e-p_w S_w)/V_P$, i.e. employing Gauss's theorem, where p_e and p_w are obtained by linear interpolation. Taking into account also the underrelaxation with the solution from the previous outer iteration, denoted by the superscript *, (4) can be written as

$$u_P=\frac{\sum_{nb}a_{nb}u_{nb}}{a_P^\alpha}+\frac{t_P}{a_P^\alpha}u_P^0+\frac{V_P}{a_P^\alpha}f_P-\frac{V_P}{a_P^\alpha}\frac{p_e S_e-p_w S_w}{V_P}+(1-\alpha_u)u_P^*, \tag{6}$$

where the summation $\sum_{nb}$ comprises neighboring points ($nb\in\{E,W,N,S\}$), α_u is the underrelaxation factor and $a_P^\alpha\equiv a_P/\alpha_u$. As we use the underrelaxation generally, the superscript $^\alpha$ is dropped hereafter for brevity.

For the calculation of mass fluxes on FV faces which are required in (5) and also in the mass conservation constraint (3) leading to the pressure field equation, the FV face velocities are necessary. Since they are not directly available on collocated grids they need to be interpolated, e.g. $u_e = I_e u_E + (1 - I_e)u_P$ so that using (6) for u_P and the corresponding equation for u_E results in

$$u_e = \widetilde{u}_e + I_e\left(\frac{t_P}{a_P}\right)_E u_E^0 + (1 - I_e)\frac{t_P}{a_P}u_P^0 + I_e\left(\frac{V_P}{a_P}\right)_E f_E + (1 - I_e)\frac{V_P}{a_P}f_P - I_e\left(\frac{V_P}{a_P}\right)_E \left.\frac{\partial p}{\partial x}\right|_E - (1 - I_e)\frac{V_P}{a_P}\left.\frac{\partial p}{\partial x}\right|_P + (1 - \alpha_u)\{I_e u_E^* + (1 - I_e)u_P^*\}, \tag{7}$$

where

$$\widetilde{u}_e = I_e\left(\frac{\sum_{nb} a_{nb}u_{nb}}{a_P}\right)_E + (1 - I_e)\frac{\sum_{nb} a_{nb}u_{nb}}{a_P}. \tag{8}$$

Analogous expressions can be obtained for u_w, v_n and v_s. Using them in (3) which on the two dimensional Cartesian grid reads

$$-u_e S_e + u_w S_w - v_n S_w + v_s S_s = 0 \tag{9}$$

leads to pressure–velocity decoupling. This is most evident on a uniform grid ($I_e = I_w = I_n = I_s = 0.5$) where values p_E, p_W, p_N and p_S cancel out and are therefore irrelevant for the satisfaction of (9).

To resolve the decoupling problem Rhie and Chow [2] suggest correcting (7) as

$$u_e \leftarrow u_e - \left(\frac{V_P}{a_P}\right)_e \left\{\left.\frac{\partial p}{\partial x}\right|_e - I_e\left.\frac{\partial p}{\partial x}\right|_E - (1 - I_e)\left.\frac{\partial p}{\partial x}\right|_P\right\}, \tag{10}$$

where $(\partial p/\partial x)_e = (p_E - p_P)/\Delta x_e$ and the coefficient $(V_P/a_P)_e$ equals

$$\left(\frac{V_P}{a_P}\right)_e = I_e\left(\frac{V_P}{a_P}\right)_E + (1 - I_e)\frac{V_P}{a_P}. \tag{11}$$

The correction (10) is very similar to replacing the interpolated pressure gradient in (7) with a directly calculated one

$$u_e \leftarrow u_e - \left(\frac{V_P}{a_P}\right)_e \left.\frac{\partial p}{\partial x}\right|_e + I_e\left(\frac{V_P}{a_P}\right)_E \left.\frac{\partial p}{\partial x}\right|_E + (1 - I_e)\frac{V_P}{a_P}\left.\frac{\partial p}{\partial x}\right|_P. \tag{12}$$

In fact, (12) and (10) are the same for a fluid with constant properties on a uniform grid. Further enhancement of (7) is proposed by Majumdar [3]

$$u_e \leftarrow u_e + (1 - \alpha_u)\{u_e^* - I_e u_E^* - (1 - I_e)u_P^*\}, \tag{13}$$

so that the converged solution does not depend on α_u. In the same manner, Choi [4] recommends

$$u_e \leftarrow u_e + \left(\frac{t_P}{a_P}\right)_e u_e^0 - I_e\left(\frac{t_P}{a_P}\right)_E u_E^0 - (1 - I_e)\frac{t_P}{a_P}u_P^0, \tag{14}$$

which results in a solution which is nearly timestep-independent, that is, Δt still affects a_P. More importantly, Yu *et al.* [13] demonstrated that using the Rhie–Chow correction without (13) and (14) can result in a checkerboard pressure field for small values of α_u and/or Δt. In another work, Yu *et al.* [6] suggest a truly Δt-independent solution; its description, however, is beyond the scope of this paper as in practice Choi's correction performs equally well.

When the fluid is subject to large body forces Gu [7] proposes

$$u_e \leftarrow u_e + \left(\frac{V_P}{a_P}\right)_e f_e - I_e\left(\frac{V_P}{a_P}\right)_E f_E - (1 - I_e)\frac{V_P}{a_P}f_P. \tag{15}$$

The corrections (12)–(15) are easily implemented by replacing (7) with

$$u_e = \widetilde{u}_e + \left(\frac{t_P}{a_P}\right)_e u_e^0 + \left(\frac{V_P}{a_P}\right)_e f_e - \left(\frac{V_P}{a_P}\right)_e \left.\frac{\partial p}{\partial x}\right|_e + (1-\alpha_u)u_e^*, \tag{16}$$

therefore reducing the task to proper identification of face value terms.

3. One-dimensional quiescent fluid subject to body forces

In this section we examine how the velocity interpolation on the FV faces affects the calculated pressure and velocity field in the presence of an abruptly variable body force. To make the analysis clear, a one-dimensional (1D) system ($x \in [x_L, x_R]$) containing two phases is considered. The distribution of phases is defined within the VOF model so that the color function C

$$C = \begin{cases} 1, & x_1 < x < x_2, \\ 0, & \text{otherwise}, \end{cases} \tag{17}$$

represents a 1D "bubble" or "drop". We consider two kinds of body force: (a) $f_g^x = g[C\rho_1 + (1-C)\rho_2]$ mimicking body force in the gravity field and (b) $f_\sigma^x = \sigma\kappa\partial C/\partial x$ resembling the CSF; as curvature is not defined in 1D κ is set manually. The velocity field of an incompressible fluid in a 1D system is uniform and determined on the boundary; we set $u = 0$ at the boundaries and accordingly seek for uniform zero velocity field solution.

Although steady state is considered in this section the calculations are transient, i.e., the timestep size Δt is set to a finite value. The convergence criteria of the timestep is defined with the condition $r_i^n/r_0^n < \varepsilon_{\Delta t}$ where r_i^n and r_0^n present norms of the residuum after the ith (outer) iteration and before the first iteration inside the nth timestep, respectively. The steady state, on the other hand, is reached when $r_0^n/r_0^1 < \varepsilon_{st}$. For the calculations in this section $\varepsilon_{\Delta t} = 1.0 \times 10^{-4}$ and $\varepsilon_{st} = 1.0 \times 10^{-10}$; Δt is set to 1.0 s unless stated otherwise.

To quantify intelligibly the magnitude of error in the solution we consider the material properties of a commonly encountered air–water system given in Table 1. The system limits x_L and x_R are set to 0.0 and 0.1 m, respectively. The "bubble" is located between $x_1 = 0.030$ m and $x_2 = 0.066$ m; the choice is such that x_1 is positioned exactly on the face of an FV on uniform grids with 20, 40 and 80 cells, whereas x_2 lies inside an FV thus considering both situations simultaneously.

The converged stationary pressure and velocity field (at the mid-FV points) in the described system subject to body force $f_P^x = g[C_P\rho_1 + (1-C_P)\rho_2]$ due to gravity $g = 1.0 \times 10^1$ m s^{-2} are drawn in Fig. 1. Figs. 1a and b display the results when the Rhie–Chow interpolation (10) is used; unphysical spikes in the velocity field are obtained. Their magnitude decreases with grid refinement but even on the uniform grid with 80 FVs they are still substantial. The result of adding Gu's correction (15) can be seen in Figs. 1c and d; the magnitude of the spikes is even larger.

The presented numerical experiment also reveals the importance of Choi's correction (14). That is, the obtained solution strongly depends on Δt if (14) is not implemented: Fig. 2a shows that the magnitude of the velocity field spikes is reduced by using smaller Δt, however, at the same time the pressure field smoothing effect is also reduced, resulting in an oscillating pressure field (Fig. 2b). This behavior agrees well with the analysis of Yu *et al.* [13]. As pointed out in the previous section, Choi's correction (14) weakens the Δt-dependence of the obtained solution (Fig. 2c). Also, the pressure field smoothing effect appears independent of Δt (Fig. 2d). Therefore, we use (14) in the calculations along with Majumdar's correction.

In order to obtain a uniform $u = 0$ solution the body force f^x should be perfectly balanced with $\partial p/\partial x$ on both the FV center points and faces. On FV faces thus $(\partial p/\partial x)_e = f_e^x$ and $(\partial p/\partial x)_w = f_w^x$ must hold, which also suits the pressure equation for quiescent fluid

$$\left(\frac{V_P}{a_P}\right)_e \left.\frac{\partial p}{\partial x}\right|_e - \left(\frac{V_P}{a_P}\right)_w \left.\frac{\partial p}{\partial x}\right|_w = \left(\frac{V_P}{a_P}\right)_e f_e - \left(\frac{V_P}{a_P}\right)_w f_w. \tag{18}$$

Table 1
Material properties of air (subscript 1) and water (subscript 2)

$\rho_1 = 1.29 \times 10^0$ kg m^{-3}	$\rho_2 = 1.0 \times 10^3$ kg m^{-3}
$\eta_1 = 1.8 \times 10^{-5}$ N s m^{-2}	$\eta_2 = 1.0 \times 10^{-3}$ N s m^{-2}
$\sigma = 7.2 \times 10^{-2}$ N m^{-1}	

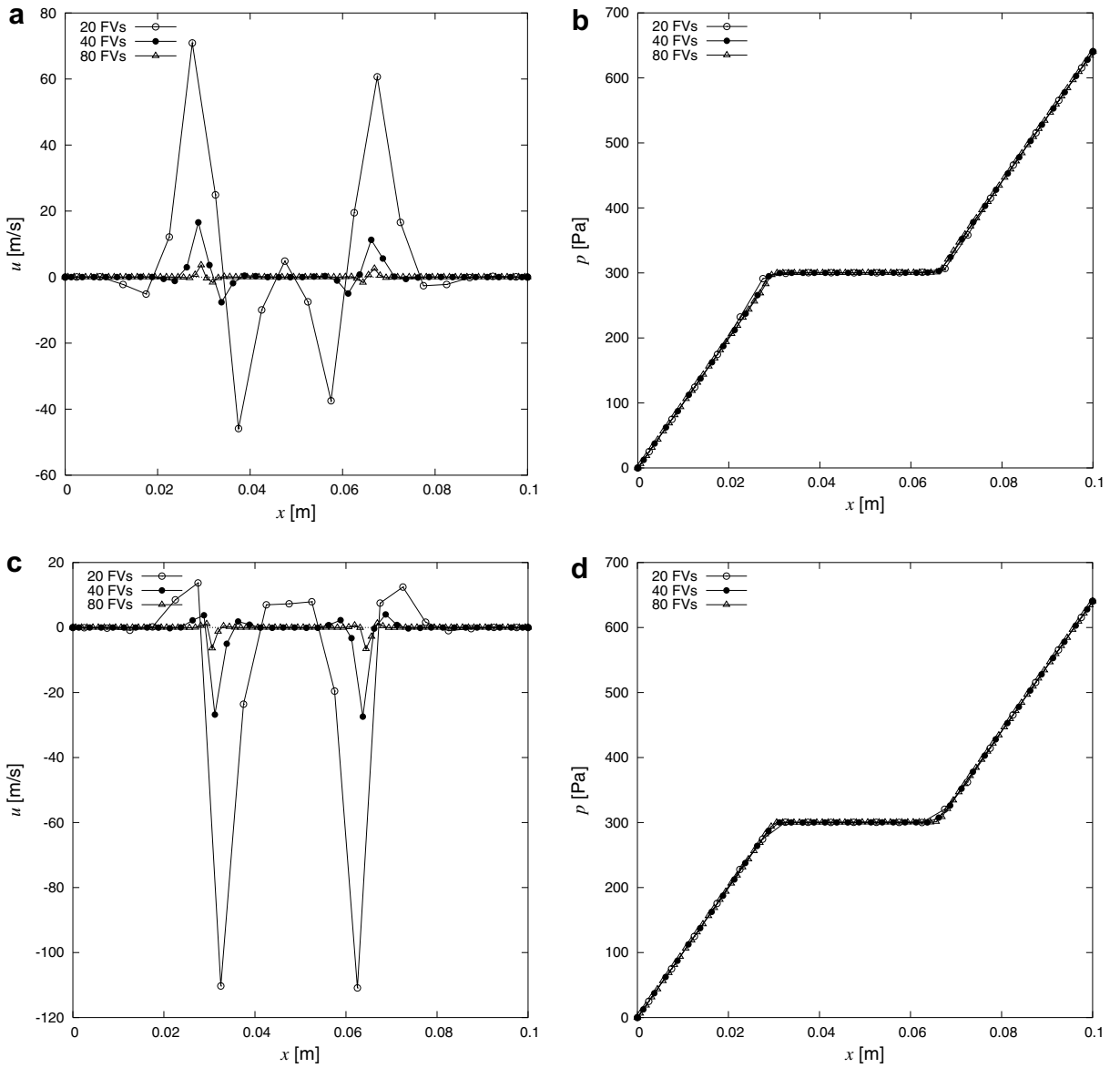

Fig. 1. Velocity and pressure field subject to gravity on uniform grids with 20, 40 and 80 FVs using the Rhie–Chow interpolation (a, b) and adding Gu's correction (c, d).

The above equation follows from (9) which on 1D grid reads $-u_e + u_w = 0$ and thus depends on the cell face velocity interpolation; (18) is obtained when both the Rhie–Chow interpolation and Gu's correction are used as in (16). If second order CDS derivative approximation is used then p_E, p_W and p_P are related as follows

$$p_E = p_P + f_e \Delta x_e \quad \text{and} \quad p_W = p_P - f_w \Delta x_w. \tag{19}$$

Considering the grid points as well, $(\partial p/\partial x)_P = f_P^x$ should hold. If Gauss's theorem is applied (where $S_e = S_w = 1$, see previous section) to calculate the derivative inside FV then

$$f_P^x = \frac{p_e - p_w}{V_P} = \frac{I_e p_E + (1 - I_e) p_P - I_w p_W - (1 - I_w) p_P}{V_P}. \tag{20}$$

Using (19) to express p_E and p_W in (20) results in the relation

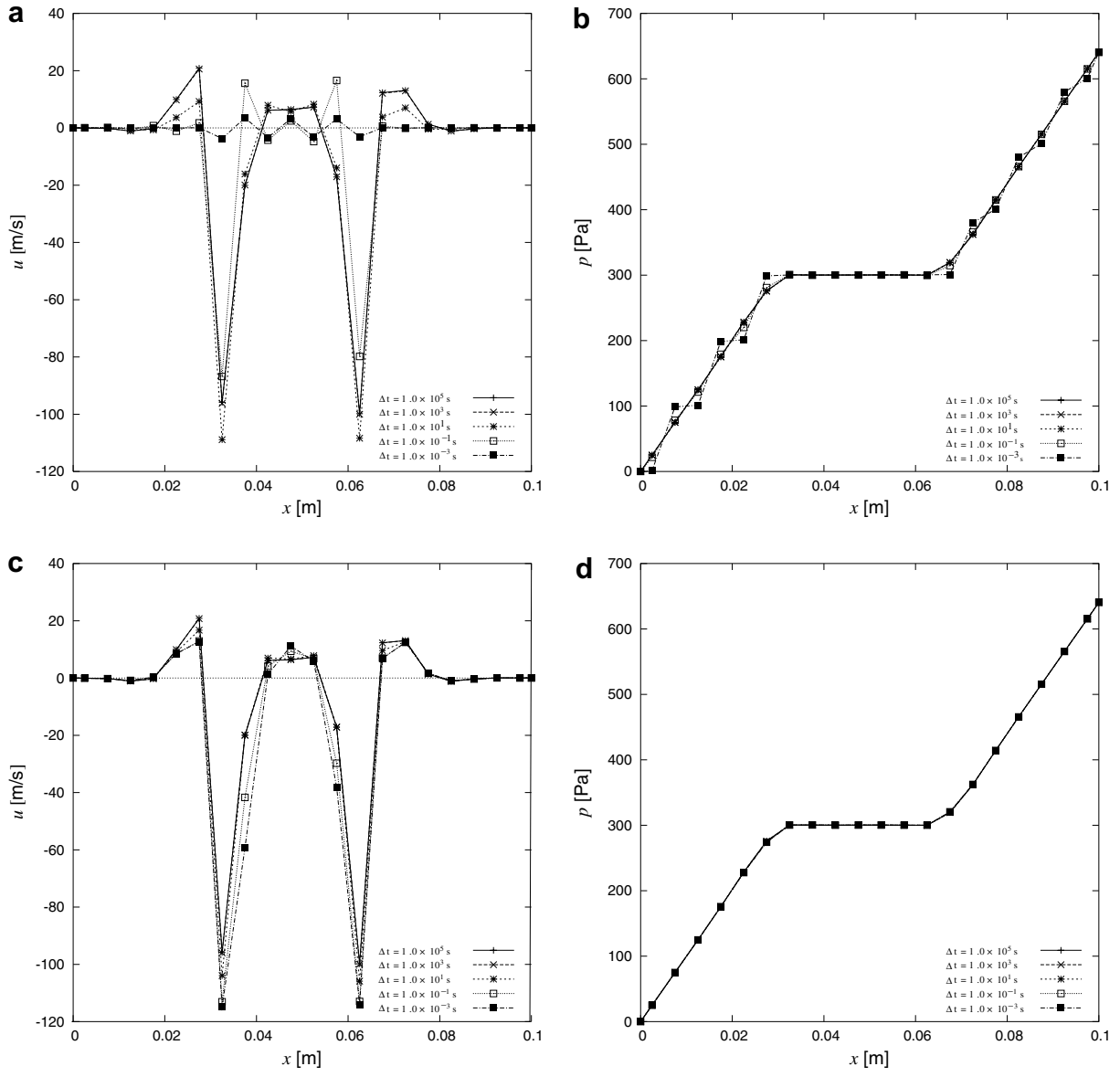

Fig. 2. Dependence on Δt of the computed velocity and pressure field subject to gravity on uniform grid with 20 FVs using Gu's correction: without (a, b) and with (c, d) Choi's correction.

$$f_P^x = \frac{I_e f_e \Delta x_e + I_w f_w \Delta x_w}{V_P}, \tag{21}$$

where, as expected, p_P cancels out. The above equation presents the *discretization rule* to obtain zero velocity at grid points if the Rhie–Chow interpolation is used with Gu's body force correction. The rule depends on the way $\partial p/\partial x$ is discretized. Nevertheless, it implies that body force should first be discretized on the FV faces and then calculated for FV. *Following this rule a machine accurate uniform $u = 0$ solution is obtained.*

Let us now consider CSF with $f_P^x = \sigma\kappa(C_e - C_w)/V_P$ where we set $\kappa = 2/(x_2 - x_1)$. The Rhie–Chow interpolation without Gu's correction again results in the spikes visible in Fig. 3. Adding Gu's correction eliminates the spikes completely because f_P^x then conforms with (21) as the discretizations of $\partial p/\partial x$ and $\partial C/\partial x$ are the same. If the latter is discretized, for example, as $(C_E - C_W)/(x_E - x_W)$ then unphysical results are again obtained on a non-uniform grid as demonstrated in Fig. 4.

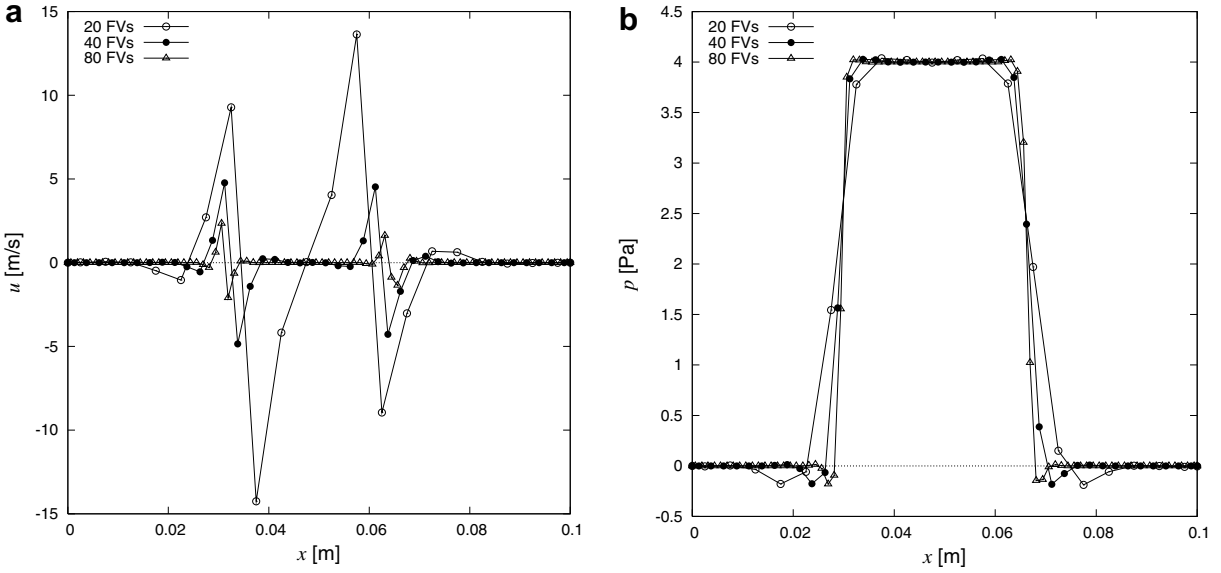

Fig. 3. Velocity and pressure field subject to CSF on uniform grids with 20, 40 and 80 FVs using the Rhie–Chow interpolation.

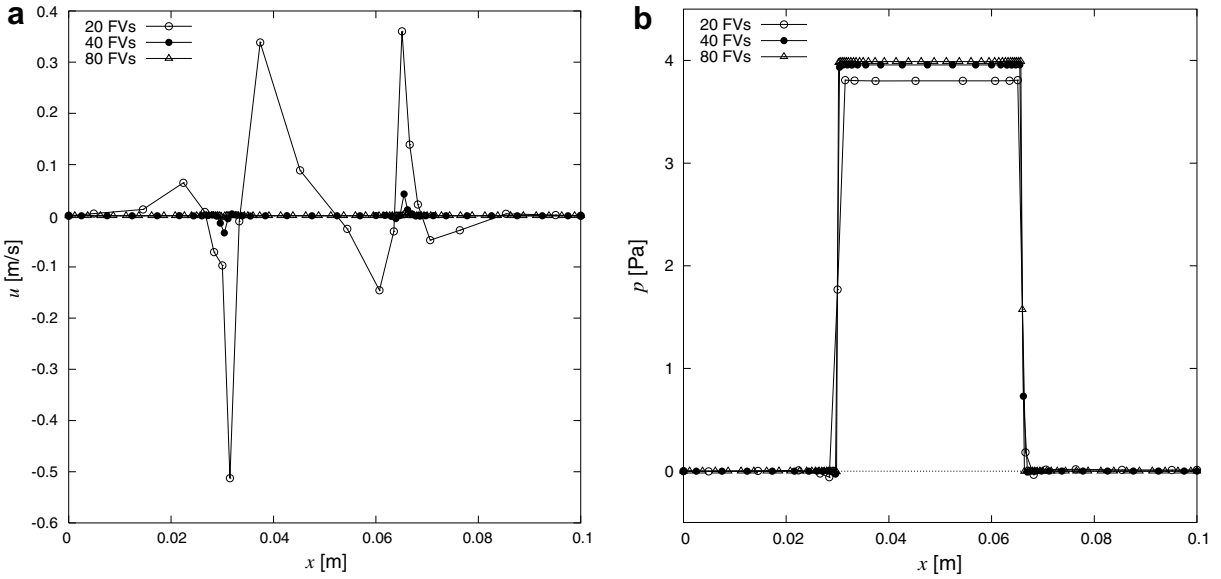

Fig. 4. Velocity and pressure field subject to CSF on non-uniform grids with 20, 40 and 80 FVs using the Rhie–Chow interpolation and Gu's correction with different discretization of $\partial p/\partial x$ and $\partial C/\partial x$.

The necessity to use the same discretization for $\partial p/\partial x$ and $\partial C/\partial x$ to eliminate spurious currents resulting from CSF was also noted by Renardy and Renardy [14] who however used staggered grids. On collocated grids this applies as well when both the Rhie–Chow interpolation and Gu's correction are used; in this case the pressure Eq. (18) is the same as on staggered grids except for the interpolated coefficients. However, it should be noted that the spurious currents considered by Renardy and Renardy which are discussed also in the next section appear on both staggered and collocated grids and are thus not related to the unphysical velocity spikes on the collocated grids.

4. Two-dimensional quiescent fluid subject to body forces

An equivalent discretization rule such as (21) can also be acquired for two- and three-dimensional problems. For simplicity we limit the discussion only to two-dimensional structured but generally non-orthogonal grids. On such a grid, (3) yields

$$G_e - G_w + G_n - G_s = 0, \tag{22}$$

where $G_e = u_e\delta y_e - v_e\delta x_e$, $G_w = u_w\delta y_w - v_w\delta x_w$, $G_n = v_n\delta x_n - u_n\delta y_n$ and $G_s = v_s\delta x_s - u_s\delta y_s$. Here, δx_f and δy_f are the components of the vector $\boldsymbol{\delta}_f$ pointing between corresponding FV-corner points as shown in Fig. 5a. Using equivalent interface interpolation as in (16) to calculate the velocity on a FV face then, for example, G_e can be written as

$$G_e = \widetilde{G}_e + \left(\frac{t_P}{a_P}\right)_e G_e^0 + \left(\frac{V_P}{a_P}\right)_e \left(f_e^x\delta y_e - f_e^y\delta x_e\right) - \left(\frac{V_P}{a_P}\right)_e \left(\left.\frac{\partial p}{\partial x}\right|_e \delta y_e - \left.\frac{\partial p}{\partial y}\right|_e \delta x_e\right) + (1-\alpha_u)G_e^*, \tag{23}$$

where

$$\widetilde{G}_e = \left[I_e\left(\frac{\sum_{nb}a_{nb}u_{nb}}{a_P}\right)_E + (1-I_e)\frac{\sum_{nb}a_{nb}u_{nb}}{a_P}\right]\delta y_e - \left[I_e\left(\frac{\sum_{nb}a_{nb}v_{nb}}{a_P}\right)_E + (1-I_e)\frac{\sum_{nb}a_{nb}v_{nb}}{a_P}\right]\delta x_e. \tag{24}$$

Expressing the derivatives in terms of computational coordinates ξ and η, (23) can be written as

$$G_e = \widetilde{G}_e + \left(\frac{t_P}{a_P}\right)_e G_e^0 + \left(\frac{V_P}{a_P}\right)_e \left(f_e^x\delta y_e - f_e^y\delta x_e\right) - \left(\frac{V_P}{a_P}\right)_e \left(\left.\frac{\alpha_e}{J_e}\frac{\partial p}{\partial \xi}\right|_e - \left.\frac{\beta_e}{J_e}\frac{\partial p}{\partial \eta}\right|_e\right) + (1-\alpha_u)G_e^{l-1}. \tag{25}$$

Here, $J_e = \Delta x_e\delta y_e - \delta x_e\Delta y_e$, $\alpha_e = \delta x_e^2 + \delta y_e^2 = |\delta_e|^2$ and $\beta_e = \delta x_e\Delta x_e + \delta y_e\Delta y_e = \boldsymbol{\delta}_e\cdot\boldsymbol{\Delta}_e$, where $\boldsymbol{\Delta}$ denotes the vectors between FV grid points as Fig. 5b shows. Inserting (25) and analogous relations for w, n and s faces in (22) gives the pressure field equation; for stagnant fluid subject to body forces it reads

$$\begin{aligned}
&\left(\frac{V_P}{a_P}\right)_e\left\{\left.\frac{\alpha_e}{J_e}\frac{\partial p}{\partial \xi}\right|_e - \left.\frac{\beta_e}{J_e}\frac{\partial p}{\partial \eta}\right|_e\right\} - \left(\frac{V_w}{a_P}\right)_w\left\{\left.\frac{\alpha_w}{J_w}\frac{\partial p}{\partial \xi}\right|_w - \left.\frac{\beta_w}{J_w}\frac{\partial p}{\partial \eta}\right|_w\right\}\\
&+\left(\frac{V_P}{a_P}\right)_n\left\{\left.\frac{\gamma_n}{J_n}\frac{\partial p}{\partial \eta}\right|_n - \left.\frac{\beta_n}{J_n}\frac{\partial p}{\partial \xi}\right|_n\right\} - \left(\frac{V_P}{a_P}\right)_s\left\{\left.\frac{\gamma_s}{J_s}\frac{\partial p}{\partial \eta}\right|_s - \left.\frac{\beta_s}{J_s}\frac{\partial p}{\partial \xi}\right|_s\right\}\\
&= \left(\frac{V_P}{a_P}\right)_e\left\{f_e^x\delta y_e - f_e^y\delta x_e\right\} - \left(\frac{V_P}{a_P}\right)_w\left\{f_w^x\delta y_w - f_w^y\delta x_w\right\} + \left(\frac{V_P}{a_P}\right)_n\left\{f_n^y\delta x_n - f_n^x\delta y_n\right\} - \left(\frac{V_s}{a_P}\right)_s\left\{f_s^y\delta y_s - f_s^x\delta y_s\right\}.
\end{aligned} \tag{26}$$

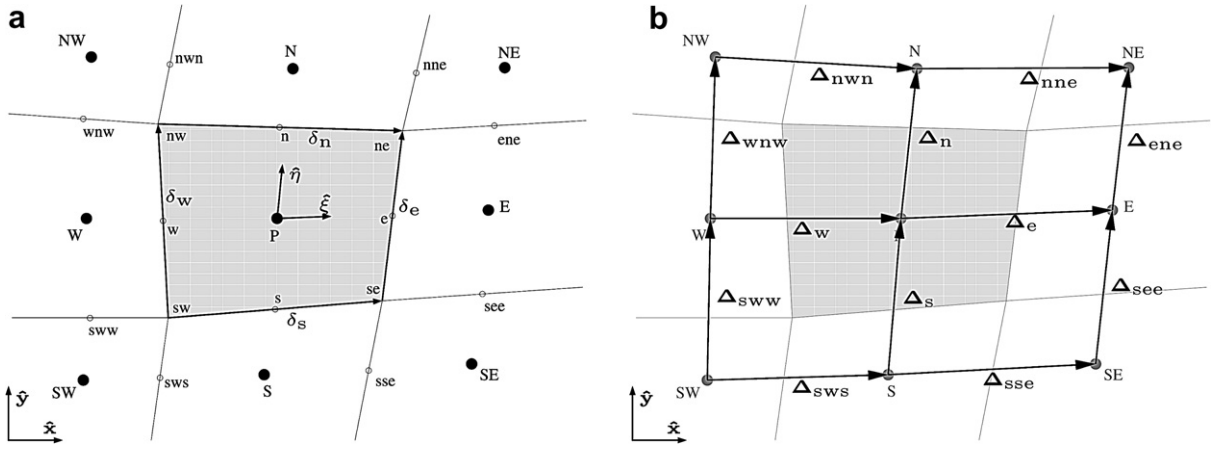

Fig. 5. Notation used on a FV grid: (a) ● – FV grid points, ○ – FV-face points, vectors $\boldsymbol{\delta} = [\delta x, \delta y]^t$ pointing between FV-corner points, (b) vectors $\boldsymbol{\Delta} = [\Delta x, \Delta y]^t$ pointing between grid points.

To obtain $G = 0$ solution on all FV faces then $\nabla p = \mathbf{f}$ should hold; replacing $\partial p/\partial x$ and $\partial p/\partial y$ with derivatives with respect to ξ and η on the e-face results in

$$\left.\frac{\partial p}{\partial \xi}\right|_e \frac{\delta y_e}{J_e} - \left.\frac{\partial p}{\partial \eta}\right|_e \frac{\Delta y_e}{J_e} = f_e^x, \quad -\left.\frac{\partial p}{\partial \xi}\right|_e \frac{\delta x_e}{J_e} + \left.\frac{\partial p}{\partial \eta}\right|_e \frac{\Delta x_e}{J_e} = f_e^y. \tag{27}$$

The solution of the above system (whose determinant equals J_e) reads

$$\begin{aligned} \left.\frac{\partial p}{\partial \xi}\right|_e &= f_e^x \Delta x_e + f_e^y \Delta y_e \Rightarrow p_E - p_P = \mathbf{f}_e \cdot \mathbf{\Delta}_e, \\ \left.\frac{\partial p}{\partial \eta}\right|_e &= f_e^x \delta x_e + f_e^y \delta y_e \Rightarrow p_{ne} - p_{se} = \mathbf{f}_e \cdot \boldsymbol{\delta}_e, \end{aligned} \tag{28}$$

which has obvious physical meaning. Analogous relations can be obtained for other FV faces. As in the previous section we also seek for a $\mathbf{u} = 0$ solution on grid points which requires $(\partial p/\partial x)_P = f_P^x$ and $(\partial p/\partial y)_P = f_P^y$. Again using Gauss's theorem to calculate derivatives in FV and linear interpolation to obtain FV face values the following is obtained:

$$\begin{aligned} f_P^x V_P = {} & \{I_e p_E + (1 - I_e) p_P\} \delta y_e - \{I_w p_W + (1 - I_w) p_P\} \delta y_w \\ & - \{I_n p_N + (1 - I_n) p_P\} \delta y_n + \{I_s p_S + (1 - I_s) p_P\} \delta y_s, \\ f_P^y V_P = {} & \{I_n p_N + (1 - I_n) p_P\} \delta x_n - \{I_s p_S + (1 - I_s) p_P\} \delta x_s \\ & - \{I_e p_E + (1 - I_e) p_P\} \delta x_e + \{I_w p_W + (1 - I_w) p_P\} \delta x_w. \end{aligned} \tag{29}$$

Inserting $p_E = p_P + \mathbf{f}_e \cdot \mathbf{\Delta}_e$ from (28) and analogous relations for other FV faces in (29) results in

$$\begin{aligned} f_P^x V_P &= I_e \delta y_e \mathbf{f}_e \cdot \mathbf{\Delta}_e + I_w \delta y_w \mathbf{f}_w \cdot \mathbf{\Delta}_w - I_n \delta y_n \mathbf{f}_n \cdot \mathbf{\Delta}_n - I_s \delta y_s \mathbf{f}_s \cdot \mathbf{\Delta}_s, \\ f_P^y V_P &= I_n \delta x_n \mathbf{f}_n \cdot \mathbf{\Delta}_n + I_s \delta x_s \mathbf{f}_s \cdot \mathbf{\Delta}_s - I_e \delta x_e \mathbf{f}_e \cdot \mathbf{\Delta}_e - I_w \delta x_w \mathbf{f}_w \cdot \mathbf{\Delta}_w, \end{aligned} \tag{30}$$

where p_P, as in (21), cancels out. The above presents the discretization rule to obtain a uniform $\mathbf{u} = 0$ field inside FV when FV face velocities are zero. The rule again depends on the discretization of ∇p. According to (30) f_P^x is expressed with both components f^x and f^y on FV faces instead of only f^x if the grid is non-orthogonal. Equivalently, f_P^y also depends on both FV face values of f^x and f^y. This discretization error originates from the use of Gauss's theorem to discretize ∇p.

In the above treatise we assumed that the solution of (26) satisfies $\nabla p = \mathbf{f}$ on all FV faces. If so, then the solution could simply be constructed using (28) and analogous relations while starting from an arbitrary grid point. Such construction of the solution must be independent of the path used. Consider, for example, four grid points P, E, N and NE (as in Fig. 5b). The difference $p_{NE} - p_P$ can be expressed as $(p_{NE} - p_E) + (p_E - p_P)$ or as $(p_{NE} - p_N) + (p_N - p_P)$; using (28) and analogous relations then

$$\mathbf{f}_{ene} \cdot \mathbf{\Delta}_{ene} + \mathbf{f}_e \cdot \mathbf{\Delta}_e = \mathbf{f}_{nne} \cdot \mathbf{\Delta}_{nne} + \mathbf{f}_n \cdot \mathbf{\Delta}_n, \tag{31}$$

must hold to allow the described construction of the solution of (26). Assuming that only one solution (up to a constant) exists we conclude that it can satisfy the discretized $\nabla p = \mathbf{f}$ equation on all FV faces only when $\mathbf{f}$ is *conservative on the discrete level* in the sense of (31). This requirement is valid also for the staggered grids.

As an illustration we consider three cases of body force allowing for quiescent fluid and test them against (31):

(1) uniform body force $\mathbf{f} = [f_c^x, f_c^y]^t$ where f_c^x and f_c^y are constants; it is easy to see that in this case $\mathbf{f}$ always satisfies (31) because $\mathbf{\Delta}_{ene} + \mathbf{\Delta}_e = \mathbf{\Delta}_{nne} + \mathbf{\Delta}_n$.
(2) body force in gravity field $\mathbf{f} = \rho[0, -g]^t$; in this case the condition (31) reads

$$\rho_{ene} \Delta x_{ene} + \rho_e \Delta x_e = \rho_{nne} \Delta x_{nne} + \rho_n \Delta x_n. \tag{32}$$

In a stratified fluid the above is met depending on the calculation of ρ on FV faces. For a two fluid system, modeled with VOF so that $\rho = \rho_1 + C(\rho_2 - \rho_1)$, ρ can be replaced with C. The condition (33)

should be satisfied when the interface is horizontal, however it depends on the calculation of C on FV faces. If a Cartesian grid ($\xi = x$ and $\eta = y$) is used then (32) further simplifies to $C_{ene} = C_n$.

(3) Continuum surface force $\mathbf{f} = \sigma\kappa\vec{\nabla}C$; in this case it is worth noting that when ∇_e is discretized, for example, as in (27) then $(\vec{\nabla}C)_e \cdot \mathbf{\Delta}_e = C_E - C_P$. Using this and analogous relations in (31) gives the zero velocity condition

$$\sigma\kappa_{ene}(C_{NE} - C_E) + \sigma\kappa_e(C_E - C_P) = \sigma\kappa_{nne}(C_{NE} - C_N) + \sigma\kappa_n(C_N - C_P). \tag{33}$$

Considering a stationary bubble we see that (33) is satisfied if κ, calculated on all relevant FV faces, is constant.

The satisfaction of (33) when CSF is considered insures a uniform $\mathbf{u} = 0$ solution; thus it must also apply for the well-known problem of the parasitic currents at the interface of a stationary bubble [11]. This problem has been investigated extensively, resulting mostly in remedies which reduce parasitic currents but do not eliminate them [15]. Jamet *et al.* [15] concluded that, at least for the second gradient method that they refer to, the essential requirement for the elimination of parasitic currents is the energy conservation achieved through careful discretization of the momentum equation. The requirement (33) applicable to CSF is much more elementary. Again, it is consistent with the argument of Renardy and Renardy [14] that the parasitic currents can be attributed solely to the finite precision of the calculation of κ as long as the discretizations of ∇p and ∇C are the same. Their key idea was that "both ∇p and ∇C are singular at the interface, but they cancel each other out". Choosing the same discretization for gradients is also natural and can thus be considered as the standard choice.

The remainder of the section is devoted to the numerical experiment dealing with the aforementioned parasitic currents problem. Renardy and Renardy [14] performed such an experiment to show that their parabolic interface reconstruction algorithm (PROST) for the calculation of κ is substantially more accurate than methods based on the relation $\kappa = \nabla \cdot \hat{\mathbf{n}}$ which thus require numerical derivation of C. Our intention, on the other hand, is to demonstrate that the parasitic currents can be eliminated only when (33) is satisfied. This can be achieved through setting $\kappa = 1/R$ which is compared against two methods to compute κ: it is either obtained with PROST [14] or from $\kappa = \nabla \cdot \hat{\mathbf{n}}$. For the latter method we follow the work of Williams *et al.* [16] so that $\hat{\mathbf{n}} = \mathbf{n}/|\mathbf{n}|$ is calculated from $\mathbf{n}(\mathbf{x}) = \int_\Omega \nabla K_8(\mathbf{x}' - \mathbf{x})C(\mathbf{x}')\mathrm{d}\mathbf{x}'$ where the kernel $K_8(\mathbf{r},\epsilon)$ is defined as

$$K_8(\mathbf{r},\epsilon) = \begin{cases} A[1 - \mathbf{r}\cdot\mathbf{r}/\epsilon^2]^4, & |\mathbf{r}| < \epsilon \\ 0, & |\mathbf{r}| \geqslant \epsilon \end{cases}; \qquad A = \frac{1}{\int_\Omega [1 - \mathbf{r}\cdot\mathbf{r}/\epsilon^2]^4 \,\mathrm{d}\mathbf{r}}. \tag{34}$$

The smoothing level parameter ϵ influences the accuracy of the method which we hereafter call WKP using the authors' initials.

The amplitude of the parasitic currents is proportional to σ/η [17]; this can be well understood as they are driven by CSF which is proportional to σ and counterbalanced by the viscous forces proportional to η. The time to reach the amplitude (which can also fluctuate in time) is proportional to fluid density ρ. We again consider air and water: an air bubble is positioned in the middle of a water-filled square cavity. The radius R of the bubble is set to 0.005 m and the side length l of the cavity to 0.02 m. Fig. 6 shows the parasitic currents on a 40×40 uniform grid obtained with the two chosen methods to calculate κ. As measures of the magnitude of the parasitic currents we use the total kinetic energy $W_k = \sum_P \rho_P |\mathbf{u}_P|^2 V_P$ and maximum velocity $u_{\max} = \max_P(|\mathbf{u}_P|)$ in the domain. Fig. 7 shows $W_k(t)$ and $u_{\max}(t)$ on 40×40, 80×80 and 160×160 uniform grids; clearly steady states are reached. Timestep size $\Delta t = 1.0 \times 10^{-4}$ s and $\varepsilon_{\Delta t} = 2.5 \times 10^{-5}$ were used for all the calculations of this case; $\epsilon = 0.005$ m was set for WKP. As expected and confirmed in Table 2, κ is calculated more accurately with PROST than with WKP. Consequently, weaker parasitic currents are induced with the former than with latter method on the same grid. Interestingly, the magnitude of the parasitic currents in the simulations with PROST on 40×40 grid and with WKP on 80×80 grid is of comparable size even though the error $|\Delta\kappa|$ differs by an order of magnitude. This could perhaps be explained by the fact that CSF acts on a smaller area when the grid is finer.

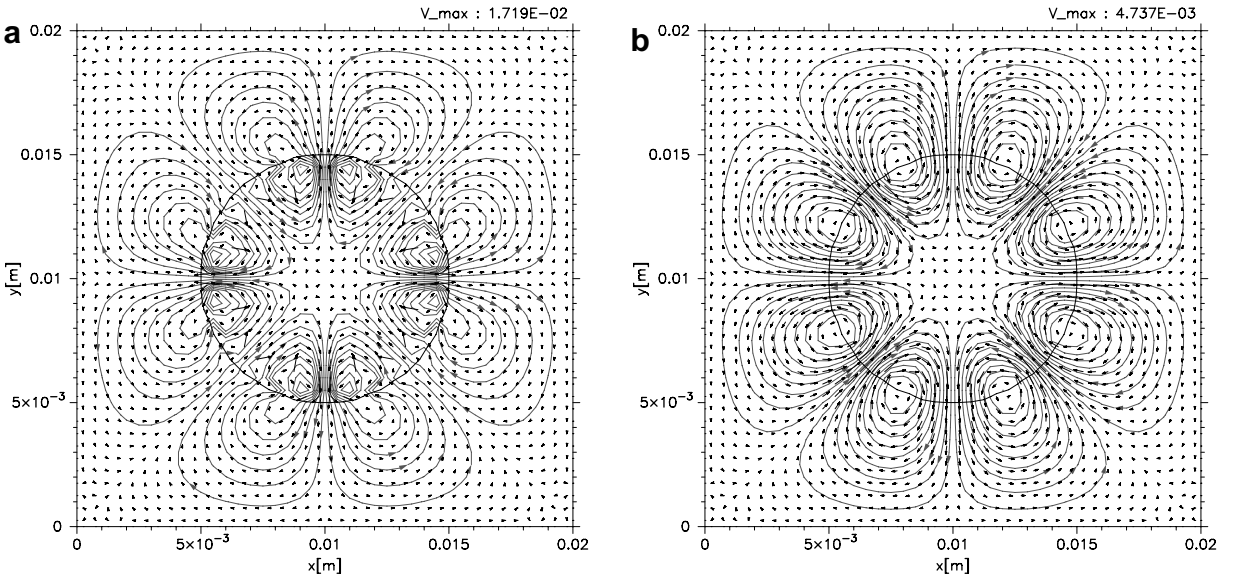

Fig. 6. Parasitic currents computed on 40×40 uniform grid for the considered case of a stationary air bubble in water: using WKP (a) and PROST (b) to obtain κ.

Also, Fig. 7 shows that the initial error, induced by the SIMPLE algorithm as the calculation is initiated with uniform pressure $p = 0$ field, reduces to round-off for exact values of κ. The presented numerical experiment confirms that parasitic currents are eliminated completely only when (33) is satisfied. Thus in practical calculations, where κ cannot be set manually, they are inevitable.

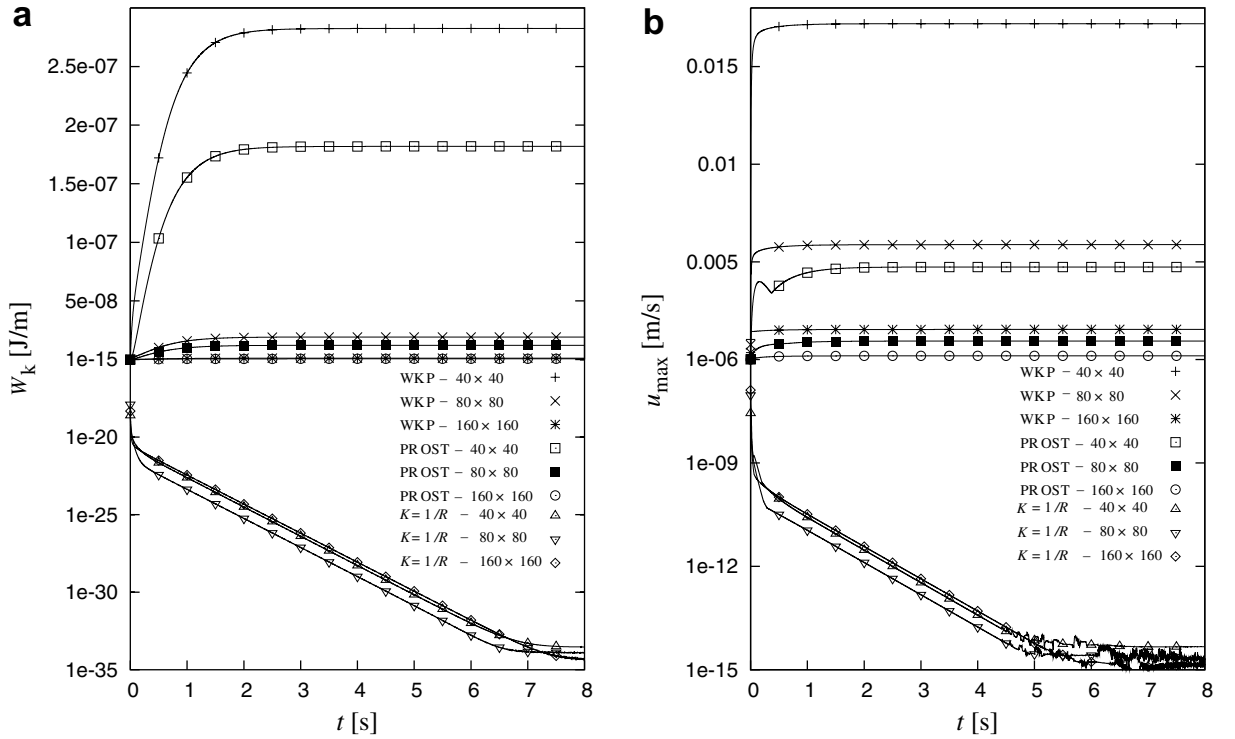

Fig. 7. $W_k(t)$ and $u_{max}(t)$ on 40×40, 80×80 and 160×160 uniform grids for the considered case of a stationary bubble using WKP, PROST and setting $\kappa = 1/R$. The vertical scales under $W_{kin} = 1.0 \times 10^{-15}$ J/m and $u_{max} = 1.0 \times 10^{-6}$ m/s on the left (a) and right (b) graphs, respectively, are logarithmic.

Table 2
Minimal and maximal error $\Delta\kappa_{\min} = \kappa_{\min} - \frac{1}{R}$ and $\Delta\kappa_{\min} = \kappa_{\min} - \frac{1}{R}$ using selected methods to obtain κ and corresponding W_k and $u_{\max}$ at $t = 8.0$ s for the considered case of a stationary bubble

Method	Grid	$\Delta\kappa_{\min}$ (m^{-1})	$\Delta\kappa_{\max}$ (m^{-1})	W_k (J/m)	$u_{\max}$ (m/s)
WKP	40×40	-2.86×10^{1}	3.56×10^{1}	2.83×10^{-7}	1.72×10^{-2}
WKP	80×80	-1.53×10^{1}	1.82×10^{1}	1.92×10^{-8}	5.88×10^{-3}
WKP	160×160	-8.43×10^{0}	8.63×10^{0}	1.03×10^{-9}	1.54×10^{-3}
PROST	40×40	6.07×10^{-1}	1.44×10^{0}	1.82×10^{-7}	4.74×10^{-3}
PROST	80×80	1.88×10^{-1}	3.75×10^{-1}	1.21×10^{-8}	9.45×10^{-4}
PROST	160×160	4.67×10^{-2}	8.90×10^{-2}	5.70×10^{-10}	1.90×10^{-4}
$\kappa = 1/R$	40×40	0.0	0.0	2.95×10^{-34}	4.65×10^{-15}
$\kappa = 1/R$	80×80	0.0	0.0	1.26×10^{-34}	2.17×10^{-15}
$\kappa = 1/R$	160×160	0.0	0.0	4.75×10^{-35}	1.15×10^{-15}

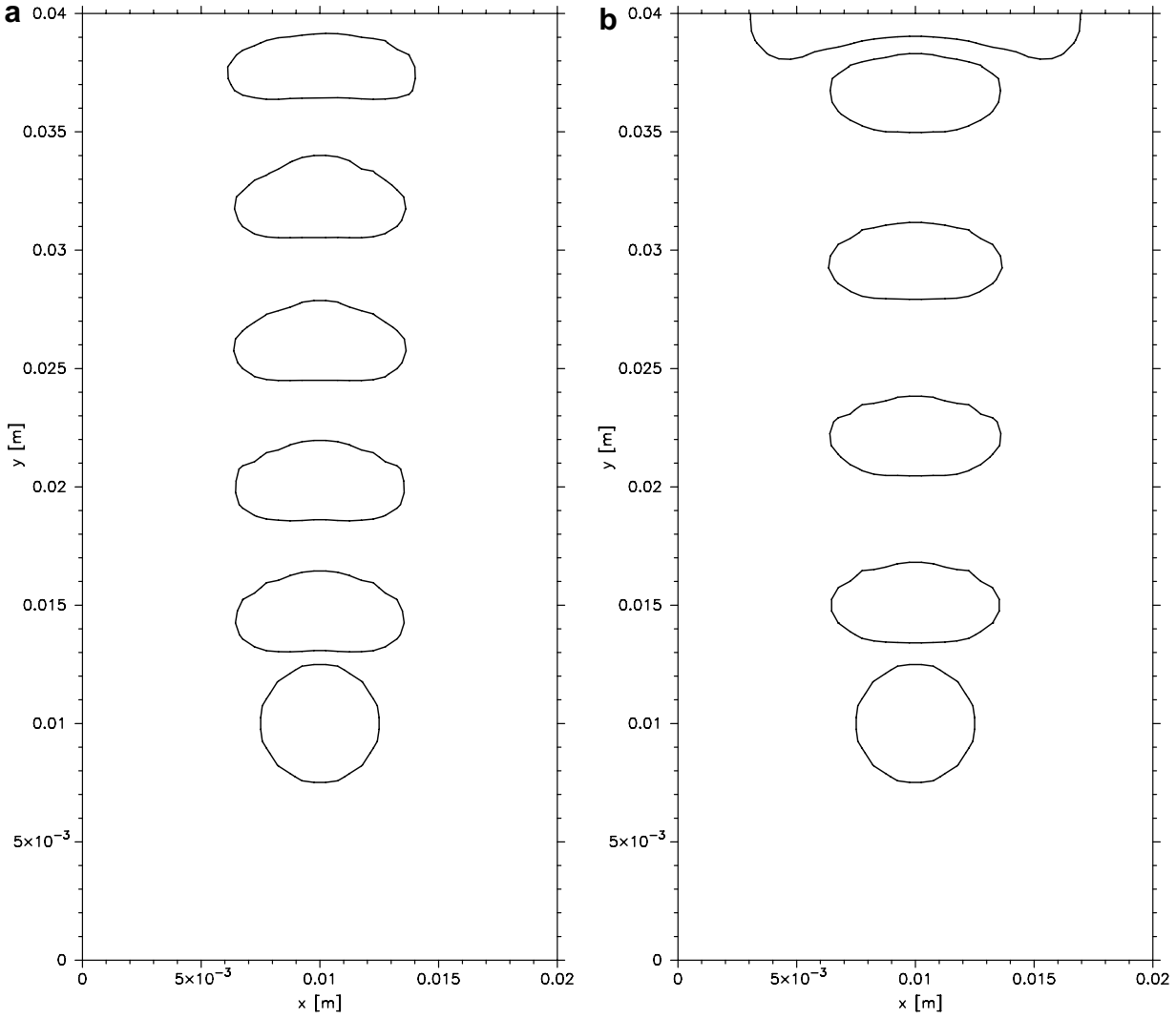

Fig. 8. Contours $C = 0.5$ at $t = 0.0$ (0.05) 0.25 s: (a) using $f_P^x = -g\rho_P$ and (b) using (30).

5. Rising bubble

The rule (30) for the discretization of body force was attained considering a stagnant fluid. To see its effect in more practical calculations, i.e. for moving fluids, we consider a two-dimensional case of a rising bubble in a rectangular cavity. Again, the material properties of air and water, given in Table 1, are used. The cavity width w and height h are set to 0.02 m and 0.04 m, respectively. No-slip boundary conditions are enforced at the walls. Initially, the round bubble with radius $R = 0.0025$ m is located at $(x_0, y_0) = (w/2, h/4)$ and the velocity field is uniformly set to zero ($\mathbf{u} = 0$).

Besides solving the Navier–Stokes equation as described earlier in the text the transport equation $\mathrm{d}C/\mathrm{d}t = 0$ must also be solved. For this purpose the CICSAM scheme of Ubbink [18] is implemented. Although the diffusion of C is not completely eliminated, this low-diffusive scheme works satisfactorily for the case presented. It turns out, however, that CICSAM is incompatible with PROST which becomes inaccurate with even weak diffusion of C – the investigation of this issue is beyond the scope of the present work. Thus, κ is calculated with WKP method [16] described in the previous section; here $\varepsilon = 5.0 \times 10^{-4}$ m. In the simulations, $\Delta t = 2.5 \times 10^{-5}$ s and $\varepsilon_{\Delta t} = 2.5 \times 10^{-5}$.

Two simulations run with the same parameters are compared. They differ only in the discretization of body force field: standard discretization $f_P^x = -g\rho_P$ is implemented in the first simulation whereas (30) is obeyed in the second one. For CSF, as explained in Section 4, standard discretization already complies with (30) and is thus the same in both simulations. Fig. 8 shows $C = 0.5$ contours indicating the position and shape of the bubble at time instants $t = 0.0\ (0.05)\ 0.25$ s calculated on 40×80 uniform grid. Both calculations in Figs. 8a and b apparently produce realistic results. A closer look at Fig. 9a reveals that unphysical spikes in the velocity field appear near the interface in the first simulation. Fig. 9b on the other hand displays the velocity field when (30) is implemented: the aforementioned spikes disappear or at least they are greatly diminished. Evidently, obeying a rule such as (30) is important.

It is interesting that despite the spikes in the velocity field, the first simulation produces reasonable results at least when looking at the contours of the bubble. This can be explained by the correcting role of the mass conservation Eq. (3). That is, the velocities on FV faces that are used for the calculation of fluxes are calculated by interpolating FV velocities and then corrected with the pressure gradient as given by (12). Nevertheless, the FV velocities still determine the FV face velocities as can be understood from (16). In the presented case therefore FV velocities near the interface regulate its movement. It is reasonable to expect that the undesired velocity spikes could in the worst case result in artificial interface instabilities or breakups.

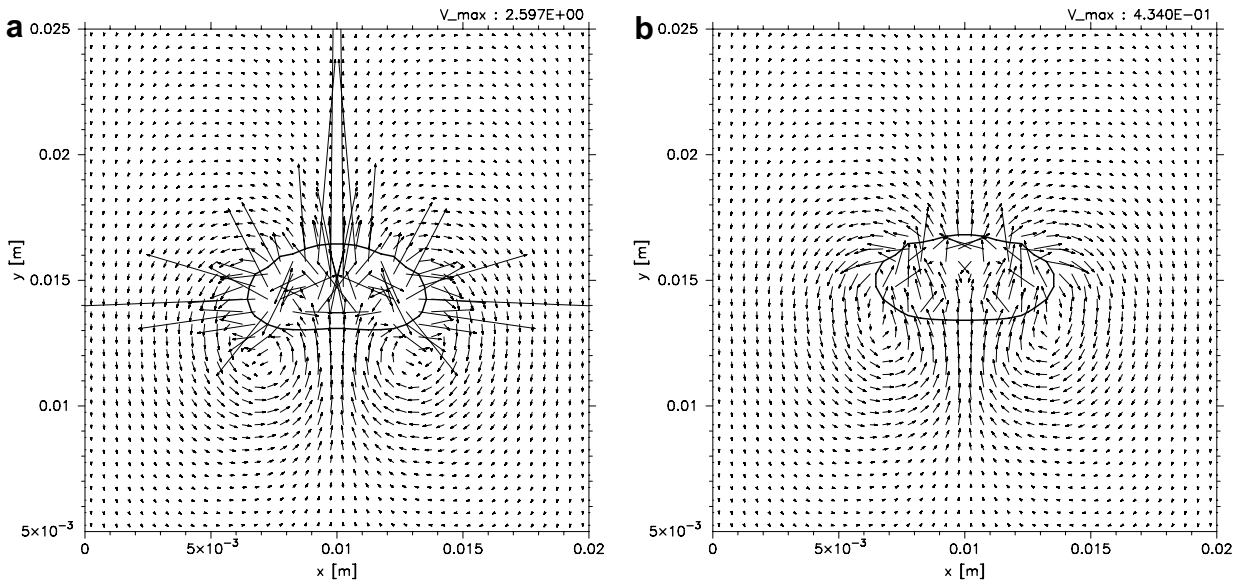

Fig. 9. Velocity field and $C = 0.5$ contour at $t = 0.05$ s: (a) using $f_P^x = -g\rho_P$ and (b) using (30).

6. Conclusions

As indicated in the paper, the FV discretization on collocated grids requires some caution when dealing with abruptly variable body force field **f**. That is, if the Rhie–Chow interpolation is used with its most important enhancements, then complying with rules such as (30) is advised in order to avoid the appearance of unphysical spikes in the velocity field near the abrupt change in **f**. The exact form of the rule depends on the discretization of ∇p, nevertheless the idea is to first compute **f** on FV faces and then use them to obtain $\mathbf{f}_P$. Such discretization does not exactly follow the spirit of the FV method where $\mathbf{f}_P$ presents the average value of **f** inside an FV, whereas in our case it is a linear combination of the average forces on FV boundaries. The difference between the two is smaller when **f** is smoother, so the proposed manner of discretization can in practice be applied generally.

The described discretization rule is obtained by imposing an additional constraint which requires a uniform $\mathbf{u} = 0$ solution where such a solution follows from physics. Such a solution, i.e., without any parasitic currents can only be obtained when the body force is conservative on the discrete level. In practical calculations this is rarely the case. Moreover, a quiescent fluid is seldom considered for practical calculations. However, it is demonstrated in Section 5 that although the proposed rule for the discretization of the force field is obtained for a quiescent fluid it can also be used for the simulations of moving fluid.

References

[1] J.H. Ferziger, M. Perić, Computational Methods for Fluid Dynamics, Springer, Berlin, 2002.
[2] C.M. Rhie, W.L. Chow, Numerical study of the turbulent flow past an airfoil with trailing edge separation, AIAA J. 21 (1983) 1525–1532.
[3] S. Majumdar, Role of underrelaxation in momentum interpolation for calculation of flow with nonstaggered grids, Numer. Heat Transfer 13 (1988) 125–132.
[4] S.K. Choi, Note on the use of momentum interpolation method for unsteady flows, Numer. Heat Transfer A 36 (1999) 545–550.
[5] J. Papageorgakopoulos, G. Arampatzisi, D. Assimacopoulos, N.C. Markatos, Enhancement of the momentum interpolation method on non-staggered grids, Int. J. Numer. Meth. Fluids 33 (2000) 1–22.
[6] B. Yu, W.-Q. Tao, J.-J. Wei, Y. Kawaguchi, T. Tagawa, H. Ozoe, Discussion on momentum interpolation method for collocated grids of incompressible flow, Numer. Heat Transfer B 42 (2002) 141–166.
[7] C.Y. Gu, Computation of flows with large body forces, in: C. Taylor, J.H. Chin (Eds.), Numerical Methods in Laminar and Turbulent Flow, Pineridge Press, Swansea, 1991, pp. 294–305.
[8] S.K. Choi, S.-O. Kim, C.-H. Lee, H.-K. Choi, Use of the momentum interpolation method for flows with large body force, Numer. Heat Transfer B 43 (2003) 267–287.
[9] J.U. Brackbill, D.B. Kothe, C. Zemach, A continuum method for modeling surface tension, J. Comput. Phys. 100 (1992) 335–354.
[10] C. Hirt, B. Nicols, Volume of fluid (VOF) method for the dynamics of free boundaries, J. Comput. Phys. 39 (1981) 201–225.
[11] B. Lafaurie, C. Nardone, R. Scardovelli, S. Zaleski, G. Zanetti, Modelling merging and fragmentation in multiphase flows with SURFER, J. Comput. Phys. 113 (1994) 134–147.
[12] S.V. Patankar, Numerical Heat Transfer and Fluid Flow, Hemisphere Publishing Corporation, 1980.
[13] B. Yu, Y. Kawaguchi, W.-Q. Tao, H. Ozoe, Checkerboard pressure predictions due to the underrelaxation factor and time step size for a nonstaggered grid with momentum interpolation method, Numer. Heat Transfer B 41 (2002) 85–94.
[14] Y. Renardy, M. Renardy, PROST: A parabolic reconstruction of surface tension for the volume-of-fluid method, J. Comput. Phys. 183 (2002) 400–421.
[15] D. Jamet, D. Torres, J.U. Brackbill, On the theory and computation of surface tension: The elimination of parasitic currents through energy conservation in the second-gradient method, J. Comput. Phys. 182 (2002) 262–276.
[16] M.W. Williams, D.B. Kothe, E.G. Puckett, Accuracy and convergence of continuum surface-tension models, in: W. Shyy, R. Narayanan (Eds.), Fluid Dynamics at Interfaces, Cambridge University Press, Cambridge, 1998, pp. 294–305.
[17] R. Scardovelli, S. Zaleski, Direct numerical simulation of free-surface and interfacial flow, Annu. Rev. Fluid Mech. 31 (1999) 567–603.
[18] O. Ubbink, Numerical prediction of two fluid systems with sharp interfaces, Ph.D. thesis, University of London, United Kingdom, 1997.